

## Magnetodielectric Properties of $\text{La}_{0.67}\text{Sr}_{0.33}\text{MnO}_3$ and $\text{Ba}_{0.7}\text{Sr}_{0.3}\text{TiO}_3$ Thin Film Heterostructures

Arjun Tarale,<sup>1</sup> Y.D. Kolekar,<sup>2</sup> V.L. Mathe,<sup>2</sup> S.B. Kulkarni,<sup>3</sup> V.R. Reddy,<sup>4</sup> and Pradeep Joshi<sup>1,\*</sup>

<sup>1</sup>School of Physical Sciences, Solapur University, Solapur, 413255, India

<sup>2</sup>Department of Physics, University of Pune, Pune, 411007, India

<sup>3</sup>Department of Physics, Institute of Science, Mumbai, 400032, India

<sup>4</sup>UGC-DAE-CSIR, Indore, 452001, India

(received date: 28 February 2012 / accepted date: 28 March 2012 / published date: August 2012)

The paper discusses synthesis and magnetodielectric properties of  $\text{La}_{0.67}\text{Sr}_{0.33}\text{MnO}_3$  (LSMO),  $\text{Ba}_{0.7}\text{Sr}_{0.3}\text{TiO}_3$  (BST), and BST/LSMO thin film heterostructures. The XRD spectra are determined for confirmation of the crystal structure of LSMO, BST and formation of a pure bi-phase composite. The paper presents variation of  $C_p$  and  $\tan\delta$  as a function of frequency between 100 Hz to 1 MHz and applied magnetic field up to 0.6 T. The observed variation of  $C_p$ ,  $\tan\delta$ , magnetocapacitance and impedance spectra are analyzed in terms of a possible equivalent circuit model. The present analysis shows that the method of impedance spectra could be used to separate out the possible contributions.

**Keywords:** magnetodielectrics, impedance spectroscopy, LSMO, BST, spin coating technique, thin film heterostructures

### 1. INTRODUCTION

Investigations of magnetodielectric (MD) systems have gained momentum in recent years, owing to the useful values of magnetocapacitance ( $M_c$ ) reported for various composites and double perovskite systems.<sup>[1-10]</sup> Here  $M_c$  is defined as  $(C_p(H)-C_p(0))/C_p(0)$ , where  $C_p(H)$  and  $C_p(0)$  are the values of parallel capacitance  $C_p$ , with and without applied magnetic field, respectively. It is observed that  $M_c$  is maximum for the systems where the ferroelectric phase and ferromagnetic/CMR phase possess the transition temperature  $T_c$  simultaneously at a particular temperature.<sup>[10]</sup> Therefore as a basic requirement one opts to select ferroelectric as well as CMR systems possessing  $T_c$  in the vicinity of room temperature.  $\text{Ba}_{1-x}\text{Sr}_x\text{TiO}_3$ ,  $\text{BaZr}_x\text{Ti}_{(1-x)}\text{O}_3$ ,  $\text{Ba}_{(1-x)}\text{Ca}_x\text{TiO}_3$ ,  $\text{BaTi}_{(1-x)}\text{Mg}_x\text{O}_3$  are the ferroelectric phases of interest. Regarding CMR materials like  $\text{La}_{(1-x)}\text{Ba}_x\text{MnO}_3$ ,  $\text{La}_{(1-x)}\text{Sr}_x\text{MnO}_3$ ,  $\text{La}_{(1-x)}\text{Ca}_x\text{MnO}_3$  have shown interesting results. It is also observed that the CMR material like  $\text{La}_{0.67}\text{Sr}_{0.33}\text{MnO}_3$  (LSMO) possesses CMR as well as large magnetostriction at  $T_c$  and therefore it is of immense interest in terms of applications as well as theoretical viewpoints.<sup>[2,10]</sup> The recent report by Zang *et al.* explores similar systems and it is observed that for BSPT/LSMO

composite thin films, the  $M_c$  is initially negative for ( $H < 0.3$  T) and then becomes positive for  $H$  up to 7 T. The negative  $M_c$  is associated to the stress induced change in dielectric constant  $\varepsilon$ , while the positive  $M_c$  occurs because of Catalan type contribution of interfacial polarization to the  $\varepsilon$ .<sup>[2,10]</sup> Thus one may select a ferroelectric material with useful values of polarization  $P$ ,  $\varepsilon$  and magnetic material with sufficient CMR effect as well as coefficient of magnetostriction  $\lambda$ .

Owing to the discussion above, the present paper reports the synthesis and magnetodielectric properties of LSMO and  $\text{Ba}_{0.7}\text{Sr}_{0.3}\text{TiO}_3$  (BST) thin film heterostructures.<sup>[7,11]</sup> The thin films are spin coated on  $\text{SiO}_2/\text{n-Si}(100)$  substrates. Here the base layer of LSMO itself is used to form the conducting bottom electrode of magnetodielectric systems.<sup>[12]</sup> Further parallel capacitance  $C_p$  and  $\tan\delta$  of heterostructures is measured by the deposition of a top electrode of 1mm diameter, forming a metal ferroelectric metal configuration. The present paper reports interesting results on  $M_c$  and the observed impedance spectra are understood in terms of a possible RC resonant circuit model.

### 2. EXPERIMENTAL

For the present studies, thin film heterostructures of LSMO and BST are deposited by employing citrate gel root (modified Pechini method) followed by spin coating tech-

\*Corresponding author: drpbjoshi@rediffmail.com  
©KIM and Springer

nique. Here hydroxide co-precipitates of the respective cations are used as starting materials. For the formation of hydroxide co-precipitates of Ba, Sr, and Ti, stoichiometric amounts of  $Ba(NO_3)_2$ ,  $Sr(NO_3)_2$  and  $K_2TiO(C_2O_4)_2 \cdot 2H_2O$  of purity > 99.9% are used as starting materials, while KOH is used as a precipitating agent. Further details of the synthesis of BST are already reported earlier.<sup>[12]</sup> Similarly LSMO is also synthesized using the modified Pechini method as discussed above. For the deposition of thin films of BST and LSMO, the concentration of citrate gel is selected to be 0.2 M/L. To determine the thickness of a single layer of spin coated thin film, a cross sectional image of two layers of LSMO + BST was obtained. It was observed that the thickness of single layers of LSMO and BST were nearly 160 nm. In the present studies LSMO and BST heterostructures were formed by depositing consecutive layers of LSMO and BST. Each heterostructure possesses two alternations of LSMO and BST. After deposition of each layer, films are pyrolyzed at 400°C, and after the deposition of each layer of LSMO or BST the heterostructure is sintered as two different batches at a temperature  $T_s$  equal to 800°C and 900°C. Two different sintering temperatures are used to understand the effect of sintering temperature on the magnetodielectric properties of the heterostructures.

### 3. RESULTS AND DISCUSSIONS

Figure 1(a), (b) and (c) show x-ray diffraction (XRD) spectra of thin films of LSMO, BST and BST/LSMO heterostructures respectively. From the Fig. 1, it could be seen that the films grown are polycrystalline in nature and all the peaks in the spectra could be accurately indexed using standard JCPDS data on the respective compositions. The LSMO is observed to exhibit the rhombohedral crystal structure with hexagonal axis of symmetry. Here the values of lattice parameters  $a$ ,  $c$  are observed to be 5.52 Å and 13.36 Å respectively, as reported earlier.<sup>[12]</sup> The BST is observed to exhibit a nearly cubic crystal structure with a signature of

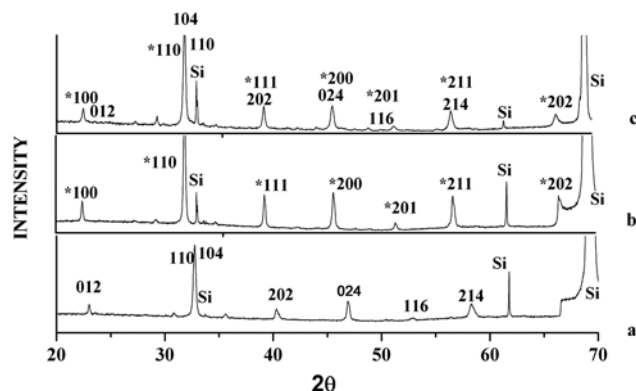


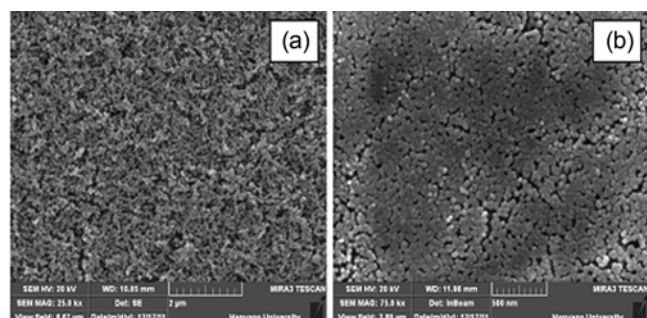
**Fig. 1.** XRD spectra of a) LSMO, b) BST, c) BST/LSMO thin film heterostructures deposited on  $SiO_2/n-Si(100)$  substrate.

mild tetragonal character and lattice parameter  $a$  (BST) = 3.97 Å<sup>[12]</sup>. The peaks in Fig. 1 are indexed with corresponding miller indices ( $h k l$ ). From the Fig. 1(c) it could be seen that in the case of BST/LSMO, the majority of the peaks of LSMO and BST overlap with each other. From the XRD spectra, it is seen that the compositions under investigation are polycrystalline and phase pure.

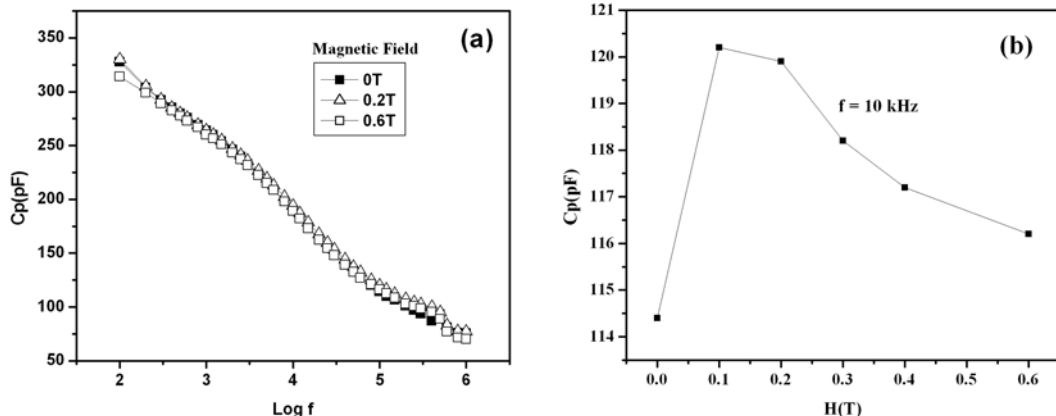
Figure 2(a), (b) show FESEM images of LSMO, BST0.3 thin films grown on  $SiO_2/n-Si(100)$  substrate. It is observed that the particles of LSMO and BST0.3 possess average grain size of nearly 50 nm. It is reported that the BST0.3, or similar thin films prepared via soft chemical route and sintered for temperature above 700°C, exhibit formation of grain growth and therefore films appear a little porous. The microstructure in Fig. 2(a) and (b) is fairly uniform and concurrent to the earlier reports.<sup>[13,14]</sup>

Figure 3(a) shows the variation of parallel capacitance  $C_p$  as a function of frequency  $f$  for applied magnetic field  $H$  equal to 0, 0.2 and 0.6 T, for BST/LSMO heterostructure sintered at 900°C. From Fig. 3(a), it is observed that for the increase in magnetic field up to 0.2 T,  $C_p$  increases with  $H$ , while for further increase in  $H$  up to 0.6 T the  $C_p$  decreases with the increase in  $H$ . This is more clear from Fig. 3(b), which shows the variation of the  $C_p$  with magnetic field at  $f = 10$  kHz. The variation of  $C_p$  with  $f$ , with varying  $H$  for the heterostructures sintered at 800°C is similar to the observations in Fig. 3. This is a typical magnetodielectric (MD) behavior. It is also known that variation of  $C_p$  as a function of  $H$  could be associated with strain induced variation of dielectric constant or variation of interfacial polarization due to the CMR effect of LSMO.<sup>[2,5,10]</sup> In fact both the contributions, one due to the CMR effect and other due to the strain induced by the giant magnetostriction of LSMO, are expected to occur simultaneously. To separate out these two contributions, one may determine impedance spectra and associate the observed variation of  $Z''$  versus  $Z'$  with possible equivalent circuit models.<sup>[15]</sup>

In addition to the variation of  $C_p$  it is also interesting to record variation of loss tangent  $\tan \delta$  as a function of frequency  $f$  and  $H$  from 0 to 0.6 T. This variation is as shown in Fig. 4 for the heterostructures sintered at 800°C. The varia-



**Fig. 2.** FESEM images of a) LSMO and b) BST thin films.



**Fig. 3.** a) Variation of capacitance  $C_p$  versus  $\log f$  for various applied magnetic fields, b) Variation of capacitance  $C_p$  versus applied magnetic field  $H$  for BST/LSMO thin film heterostructure at  $f = 10$  kHz ( $T_s = 900^\circ\text{C}$ ).

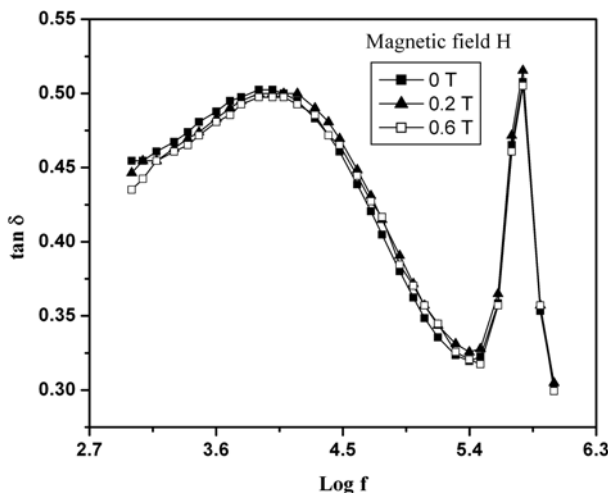


**Fig. 4.** Variation of  $\tan \delta$  versus  $\log f$  for various applied magnetic fields for BST/LSMO thin film heterostructures ( $T_s = 800^\circ\text{C}$ ).

tion of  $\tan \delta$  as a function of  $f$  for the heterostructures sintered at  $900^\circ\text{C}$  is similar in nature with variation shown in Fig. 4. It is observed that the  $\tan \delta$  passes through a resonance peak in the vicinity of 50 kHz, which is typical of BST or similar compositions.<sup>[2,11]</sup> It is also observed that the  $\tan \delta$  passes through a sharp peak in the vicinity of 500 kHz, which may correspond to the electromechanical resonance frequency for the radial mode of the oscillations. Further, the application of the magnetic field causes the resonance peak in  $\tan \delta$  to shift slightly towards the lower frequency side. Nevertheless, instead of analyzing the variation of  $\tan \delta$  and  $C_p$  separately, it is convenient to understand the variation of  $Z''$  versus  $Z'$ .

Before we analyze impedance spectra let us look at the variation of  $Mc$  with  $f$  and  $H$ . Table 1 shows values of  $Mc$  at various frequencies for the heterostructures sintered at  $800^\circ\text{C}$  and  $900^\circ\text{C}$ . It is observed for  $H$  up to 0.2 T the  $Mc$  is positive, while for the magnetic field between 0.2 to 0.6 T

**Table 1.** Variation of positive magnetocapacitance ( $Mc-1$ ) and negative magnetocapacitance ( $Mc-2$ ) for BST/LSMO heterostructures and sintering temperature  $T_s = 800^\circ\text{C}$  and  $T_s = 900^\circ\text{C}$ .

Freq. $f$ (kHz)	$Mc-1$ ( $T_s = 800^\circ\text{C}$ )	$Mc-2$ ( $T_s = 800^\circ\text{C}$ )	$Mc-1$ ( $T_s = 900^\circ\text{C}$ )	$Mc-2$ ( $T_s = 900^\circ\text{C}$ )
0.1	-	-	0.7	-4.9
1	1.2	-2.8	0.1	-1.5
10	2.5	-3.0	2.4	-2.5
100	1.6	-2.6	4.9	-3.2
500	1.2	-2.0	2.2	-6.5
1000	1.0	-3.9	2.1	-9.0

the  $Mc$  is negative for all the frequencies. The positive and negative values of  $Mc$  are being represented as  $Mc-1$  and  $Mc-2$  respectively. It is observed that the  $Mc$  shows an increasing trend as the frequency increases. The positive value of  $Mc$  is associated with the Catalan type contribution, while the negative value of  $Mc$  is expected to occur because of induced stress.<sup>[1,2,5,6]</sup> For the heterostructure sintered at  $900^\circ\text{C}$ , the maximum value of magnetic tunability,  $Mc$ , is observed to be -9%, while for that sintered at  $800^\circ\text{C}$ , it is -3.9%. It would be interesting to associate these variations with a particular effect only after impedance spectra is analyzed.

Figure 5 shows the observed impedance spectra for the heterostructure sintered at  $900^\circ\text{C}$  with varying  $H$ . The spectrum for the heterostructure sintered at  $800^\circ\text{C}$  is similar to Fig. 5. From inspection of Fig. 5 and the impedance spectra as discussed in an earlier report on simulation, it appears that the dielectric properties of the heterostructures could be represented as two parallel RC circuits connected in series with a capacitance  $C_i$ .<sup>[4,15]</sup> Figure 6 shows the required equivalent circuit for MD heterostructures, comprised of  $R_1$  |  $C_1$ ,  $R_2$  |  $C_2$  and  $C_i$  all connected in series. Here the  $R_1$ ,  $C_1$ , represent low frequency semicircle at  $\omega_{01}$ , while  $R_2$ ,  $C_2$  represents a

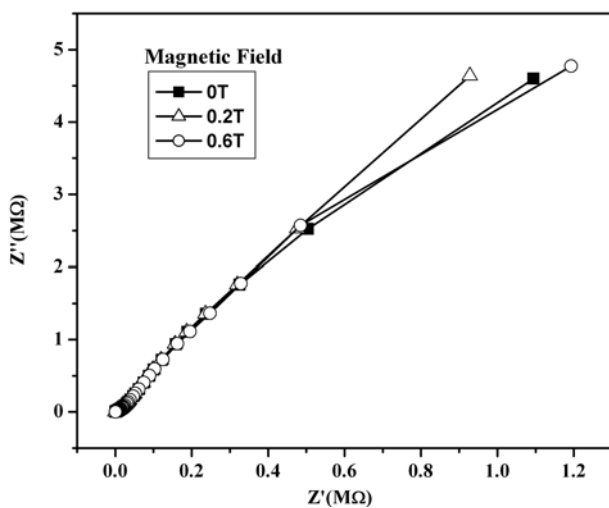


**Fig. 5.** Observed variation of complex impedance  $Z''$  versus  $Z'$  for various applied magnetic fields for BST/LSMO thin film heterostructures ( $T_s = 900^\circ\text{C}$ ).

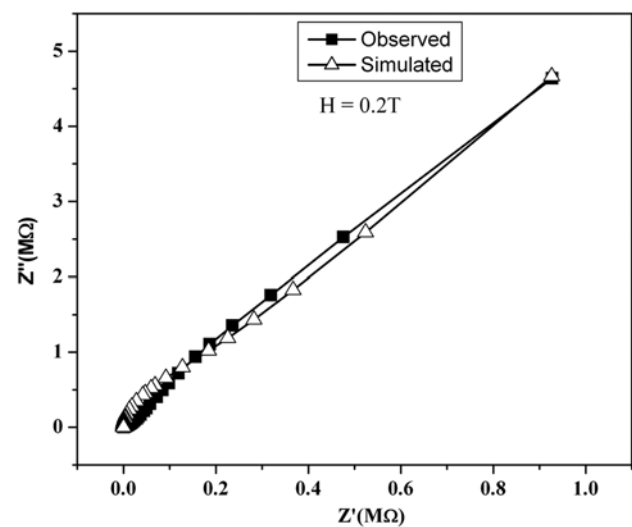


**Fig. 7.** Observed and simulated variation of complex impedance  $Z$  versus  $Z'$  for BST/LSMO thin film at the applied magnetic field equal to 0.2 T.

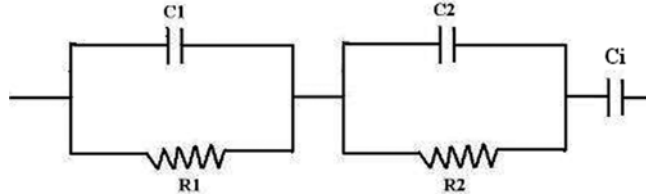


**Fig. 6.** Equivalent circuit model for MD thin film heterostructures.

high frequency resonant circuit at  $\omega_{02}$  and  $C_i$  represents capacitance due to interfacial polarization. High and low frequency semicircles occur because of heterogeneity of acceptor states in the bulk and grain boundaries of BST grains or other similar titanate compositions.<sup>[16,17]</sup> The  $C_i$  is interfacial capacitance due to the difference in the resistivity and dielectric constant of the LSMO and BST layers. A similar contribution is already modeled by Catalan.<sup>[1]</sup> For the purpose of simulation of the impedance spectra  $C_i$  is determined by making use of the data at low frequencies, while the values of  $R_1$ ,  $C_1$ ,  $\omega_{01}$  and  $R_2$ ,  $C_2$ ,  $\omega_{02}$  are determined after subtracting this contribution from the observed impedance spectra. Table 2 shows the values of  $R_1$ ,  $C_1$ ,  $\omega_{01}$ ,  $R_2$ ,  $C_2$ ,  $\omega_{02}$  and  $C_i$  for

the heterostructures investigated in the present case. The magnitudes of  $R_1$ ,  $C_1$ ,  $R_2$ ,  $C_2$  and  $C_i$  are calculated so that the observed and simulated curves closely match with each other with maximum possible accuracy. Both the observed as well as simulated impedance spectra for heterostructures sintered at  $900^\circ\text{C}$  with 0.2 T applied magnetic field are shown in Fig. 7.

From Table 2 it is seen that for the sintering temperature of  $800^\circ\text{C}$  the variation in  $R_1$ ,  $C_1$ , or  $R_2$ ,  $C_2$  or  $C_i$  are comparable but low, and it is expected that both the Catalan type and stress induced effect in polarization are equivalent for these heterostructures. This may lead to very low values of  $M_c$ . This feature could be confirmed from the observations in Table 1. For low sintering temperature the tetragonality of BST could be low and may lead to lower values of  $\epsilon$  per unit cell. Further for the annealing temperature of  $900^\circ\text{C}$  the  $R_1$ ,  $C_1$  vary significantly as compared to the variation in  $C_i$ . Therefore the strain induced contribution to  $M_c$  would be significant. From the magnitude of  $C_i$  for the samples annealed at  $800^\circ\text{C}$  and  $900^\circ\text{C}$ , it is observed that the  $C_i$  reduces with increasing annealing temperature. From Table

**Table 2.** Variation of the impedance parameters for BST/LSMO heterostructure sintered at  $800^\circ\text{C}$  and  $900^\circ\text{C}$  for various applied magnetic field H.

Sintering Temp. (°C)	H (T)	$R_1$ (M $\Omega$ )	$C_1$ (pF)	$\omega_{01}$ (Rad/Sec)	$R_2$ (M $\Omega$ )	$C_2$ (pF)	$\omega_{02}$ (Rad/Sec)	$C_i$ (pF)
800	0	0.084	947	12560	0.04	199	75360	955
800	0.6	0.086	925	12560	0.04	199	75360	780
900	0	1.52	1047	628	0.32	829	3768	420
900	0.2	1.27	1253	628	0.30	884	3768	400
900	0.6	1.61	989	628	0.40	663	3768	400

II it is seen that the  $C_i$  decreases with the increase in magnetic field  $H$ . This observation suggests that the contribution of interfacial polarization, i.e.  $Z'' = 1/(\omega C_i)$ , is more for increased sintering temperature. This feature may occur because of the reduction of interfaces between LSMO and BST as the sintering temperature increases. It is also known that for greater Catalan type contribution the  $M_c$  would be less negative or positive, while for the greater contribution of stress induced polarization  $M_c$  would be more negative. Therefore, as the contribution due to stress induced effect is greater, the comparative magnitude of  $M_c$  is expected to be larger and negative. The magnitudes of  $M_c$  in Table 1 are concurrent with the qualitative predictions made above. Thus in the case of BST the stress induced effect, i.e. Gridnev type contribution, dominates over the Catalan type contribution.<sup>[1,5]</sup> Thus it is seen that the above contributions could be separated out using the present equivalent circuit model as shown in Fig. 6.

#### 4. CONCLUSIONS

The present studies show that the analysis of impedance spectra could be used to separate out the Catalan type and Gridnev type contributions to the dielectric constant. Further, the analysis may provide guidelines for the design of various heterostructures possessing large positive or negative magnitudes of  $M_c$ .

#### ACKNOWLEDGEMENTS

The authors here by acknowledge with thanks the help rendered by Dr. R. C. Pawar, Prof. S. C. Lee (Div. of Materials and Chemical Engineering Hanyang University Ansan, 426-791, South Korea) and Dr. M. Gupta (UGC-DAE-CSR Indore (M.P.), India) for providing FESEM images and XRD spectra of the thin films.

#### REFERENCES

1. G. Catalan, *Appl. Phys. Lett.* **88**, 102902 (2006).
2. S. Zhang, X. Dong, Y. Chen, G. Wang, J. Zhu, and X. Tang, *Solid State Communications* **151**, 982 (2011).
3. S. Zhang, X. Dong, F. Gao, Y. Chen, F. Cao, J. Zhu, X. Tang, and G. Wang, *J. Appl. Phys.* **110**, 046103 (2011).
4. N. G. Kim, Y. S. Koo, C. J. Won, N. Hur, and J. H. Jung, *J. Appl. Phys.* **102**, 014107 (2007).
5. S. A. Gridnev, A. V. Kalgin, and V. A. Chernykh, *Ferroelectrics* **109**, 70 (2009).
6. M. P. Singh, K. D. Truong, and P. Fournier, *Appl. Phys. Lett.* **91**, 042504 (2007).
7. Y. Hou, Q. X. Yu, Y. P. Yao, X. H. Huang, S. N. Dong, Y. Chen, and X. G. Li, *Ferroelectrics* **409**, 196 (2010).
8. Y. S. Koo, T. Bonaedy, K. D. Sung, J. H. Jung, J. B. Yoon, Y. H. Jo, M. H. Jung, H. J. Lee, T. Y. Koo, and Y. H. Jeong, *Appl. Phys. Lett.* **91**, 212903 (2007).
9. J. H. Park, H. M. Jang, H. S. Kim, C. G. Park, and S. G. Lee, *Appl. Phys. Lett.* **92**, 062908 (2008).
10. T. Bonaedy, K. M. Song, K. D. Sung, N. Hur, and J. H. Jung, *Solid State Communication* **148**, 424 (2008).
11. A. Ianculescu, D. Berger, L. Mitoşeriu, C. E. Ciomaga, G. Voicu, N. Dragan, D. Crişan, and E. Vasile, *Ferroelectrics* **369**, 22 (2008).
12. A. N. Tarale, S. R. Jigajeni, D. J. Salunkhe, P. B. Joshi, S. B. Kulkarni, D. M. Phase, R. J. Chaudhary, and S. K. Deshapande, *J. Mater. Sci.: Mater. Electron.* **23**, 557 (2012).
13. F. M. Pontes, E. Longo, E. R. Leite, and J. A. Varela, *Thin Solid Films* **386**, 91 (2001).
14. J. Zhai, X. Yao, and H. Chen, *Ceramic International* **30**, 1237 (2004).
15. L. Pandey, Om Parkash, R. K. Katare, and D. Kumar, *Bull. Mater. Sci.* **18**, 563 (1995).
16. Om Parkash, C. D. Prasad, and D. Kumar, *J. Phys. D: Appl. Phys.* **27**, 1509 (1994).
17. Om Parkash, D. Kumar, and C. C. Christopher, *Proc. Indian Acad. Sci. (Chem. Sci.)* **115**, 649 (2003).